ARTICLE

Nanoparticles That Sense Thrombin Activity As Synthetic Urinary Biomarkers of Thrombosis

Kevin Y. Lin,[†,◆] Gabriel A. Kwong,[‡,§,◆] Andrew D. Warren,[‡,§] David K. Wood,[‡,§,⊥] and Sangeeta N. Bhatia[‡,§,∥,#,▽,⊗,*]

[†]Department of Chemical Engineering, Massachusetts Institute of Technology, Cambridge, Massachusetts 02139, United States, [‡]Harvard—MIT Division of Heath Sciences and Technology, Massachusetts Institute of Technology, Cambridge, Massachusetts 02139, United States, [§]Institute for Medical Engineering and Science, Massachusetts Institute of Technology, Cambridge, Massachusetts 02139, United States, [⊥]Department of Biomedical Engineering, University of Minnesota, Minneapolis, Minnesota 55455, United States, [∥]Electrical Engineering and Computer Science, David H. Koch Institute for Integrative Cancer Research, Massachusetts Institute of Technology, Cambridge, Massachusetts 02139, United States, [#]Broad Institute of Harvard and MIT, Cambridge, Massachusetts 02139, United States, [▽]Department of Medicine, Brigham and Women's Hospital, Boston, Massachusetts 02115, United States, and [⊗]Howard Hughes Medical Institute, Cambridge, Massachusetts 02139, United States. [◆]K. Y. Lin and G. A. Kwong contributed equally.

ABSTRACT Thrombin is a serine protease and regulator of hemostasis that plays a critical role in the formation of obstructive blood clots, or thrombosis, that is a life-threatening condition associated with numerous diseases such as atherosclerosis and stroke. To detect thrombi in living animals, we design and conjugate thrombin-sensitive peptide substrates to the surface of nanoparticles. Following intravenous infusion, these "synthetic biomarkers" survey the host vasculature for coagulation and, in response to substrate cleavage by thrombin, release ligand-encoded reporters into the host urine. To detect the urinary reporters, we develop a companion 96-well immunoassay that utilizes antibodies to bind specifically to the ligands, thus capturing the reporters for quantification. Using a thromboplastin-induced mouse model of pulmonary embolism, we show that urinary biomarker levels differentiate between healthy and thrombotic states and correlate closely with the aggregate burden of clots formed in the lungs. Our results demonstrate that synthetic biomarkers can be engineered to sense vascular diseases remotely from the urine and may allow applications in point-of-care diagnostics.

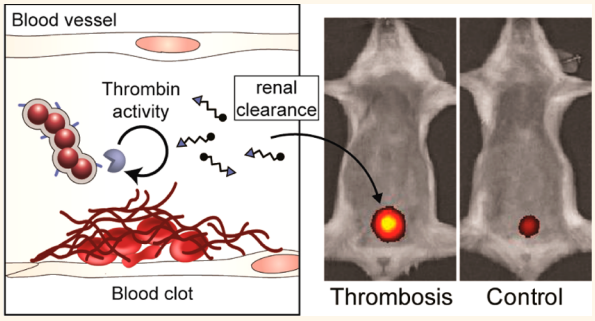

KEYWORDS: synthetic biomarkers · nanoparticles · peptides · thrombin · urinary diagnostic

Urine analysis has a rich and long-standing clinical history as a tool for monitoring health and disease and remains an integral component of a medical examination.[1−3] Well over 100 tests can be performed to indicate conditions as diverse as pregnancy,[4,5] diabetes,[6−9] kidney diseases,[10−12] metabolic disorders,[13,14] and others. Recently, the discovery of urinary analytes that were previously thought to be present mainly in circulating blood because of their large hydrodynamic radii (*e.g.*, enzymes, exosomes and others) has expanded the diagnostic repertoire to include urinary biomarkers against diseases of distant organs such as breast and brain cancer.[15,16] Inspired by the elegant physiology of the renal system, which has evolved the capacity to selectively filter liters of blood to remove byproducts of biological processes within minutes, we recently developed a class of protease-sensitive nanoparticles, called "synthetic biomarkers", that in response to dysregulated protease activity at the sites of disease, release reporters into the circulation that are then concentrated into the host urine for noninvasive monitoring.[17] In murine models of liver fibrosis and cancer, we showed that synthetic urinary biomarkers have the potential to noninvasively monitor solid organs and improve early stage detection of cancer compared to tumor-secreted blood biomarkers.

Here we hypothesized that synthetic biomarkers could be tailored to survey intravascular sites for acute thrombosis, the activation of a cascade of protease activity that orchestrates the formation of obstructive

* Address correspondence to sbhatia@mit.edu.

Received for review July 11, 2013 and accepted September 9, 2013.

Published online September 09, 2013
10.1021/nn403550c

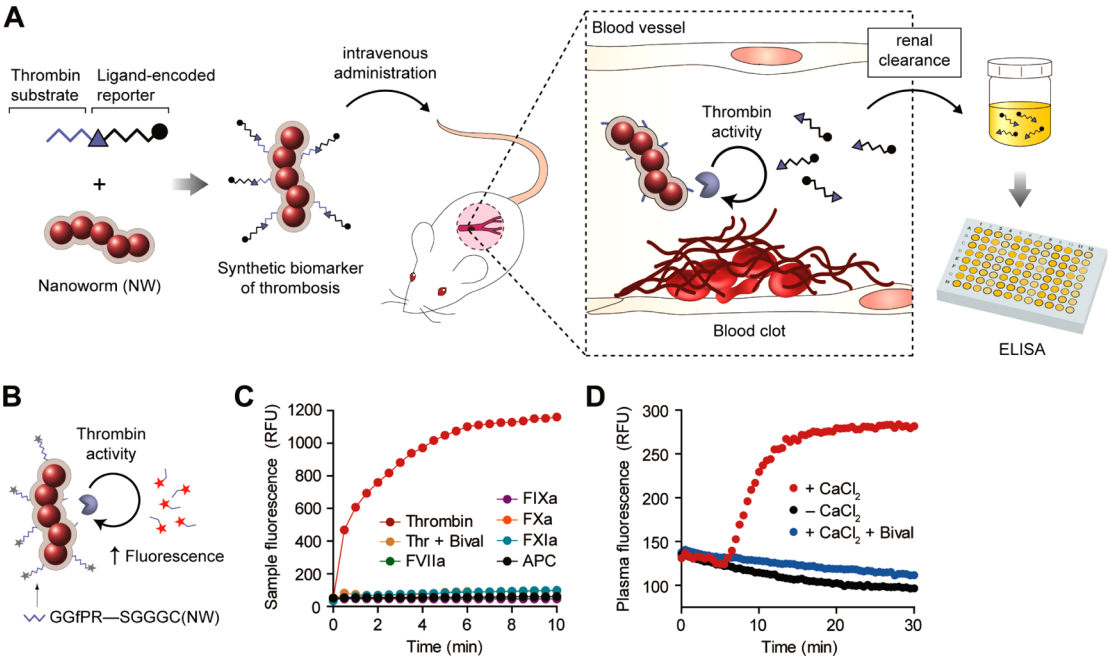

Figure 1. (A) Schematic of approach. Synthetic biomarkers composed of NWs conjugated with a thrombin-sensitive substrate in tandem with a ligand-encoded reporter. These agents survey the vasculature for the sites of clot formation where thrombin activity cleaves and releases the reporters into urine for analysis by ELISA. (B) Schematic of fluorogenic NW assay for detecting protease activity. (C) Kinetics of fluorogenesis produced by the activity of thrombin (red) and other coagulation proteases (n = 3 per condition). Thr, thrombin; Bival, bivalirudin. (D) Kinetics of fluorogenesis in plasma after the addition of $CaCl_2$ to activate coagulation (n = 3 per condition).

blood clots within vessels (Figure 1A). Thrombi are a critical pathophysiological feature of numerous vascular diseases including acute coronary syndrome, stroke, and venous thromboembolism.[18] The most important serine protease in the coagulation cascade is thrombin, which not only catalyzes the conversion of fibrinogen to fibrin that serves as the structural scaffold of a clot, but also regulates hemostasis through positive and negative feedback circuits.[19,20] To date, a number of studies have described the use of near-infrared fluorogenic probes to detect thrombin activity in the setting of thrombus formation as well as other thrombin-dependent diseases such as atherosclerosis.[21−23] More recently, these probes have been modified to include cell penetrating mechanisms that are activated after cleavage to improve the retention of the imaging agent and maintenance of the detection signal.[23,24] In the clinic, blood biomarkers such as prothrombin fragment 1.2 (a byproduct of prothrombin cleavage into thrombin) and D-dimer (a byproduct of fibrin degradation) are often used as indicators of thrombosis; however, these tests are highly susceptible to artifacts introduced by a blood draw, have poor specificity, and more accurately reflect upstream or downstream cleavage events (*i.e.*, Factor Xa activation of prothrombin or plasmin activity during fibrinolysis, respectively) rather than thrombin activity.[25−27] In this report, we engineer nanoparticles that survey the host vasculature for thrombi and,[17,28] in response to thrombin activity, release reporters into the urine as an integrated measure of the aggregate burden of systemic clots. We describe a method to encode these reporters with structurally distinct ligands that allow antibody-based detection by enzyme-linked immunosorbent assay (ELISA) in standardized 96-well plates that makes this platform readily amenable for use in clinical laboratories.

RESULTS AND DISCUSSION

Engineering Thrombin-Sensitive Synthetic Biomarkers. The construction of synthetic biomarkers for thrombosis involves modifying the surface of iron oxide nanoworms (NW), a nanoparticle formulation previously developed by our collaborators,[29,30] with substrate-reporter tandem peptides that are cleavable by thrombin and detectable by ELISA (Figure 1A). NWs were chosen for their safety profile and large hydrodynamic diameter (~40 nm, Figure S1A, Supporting Information), which prevents surface-conjugated peptides from filtering directly into the urine (~5 nm glomerulus size-exclusion limit) before cleavage.[17,28] To first develop a suitable substrate, we extended the thrombin cleavable sequence fPR−x−S (x = site of cleavage, $k_{cat}/K_m \sim 9.33 \times 10^6$)[31−34] to include glycine spacers and a C-terminal cysteine to allow coupling to NWs *via* sulfhydryl chemistry.[30] To test substrate specificity, we conjugated fluorophore-labeled derivatives onto NWs (sequence = (K-Flsc)GGfPRSGGGC, Figure S2A, Supporting Information) at a valency (~40 peptides per NW by absorbance spectroscopy, Figure S1B,

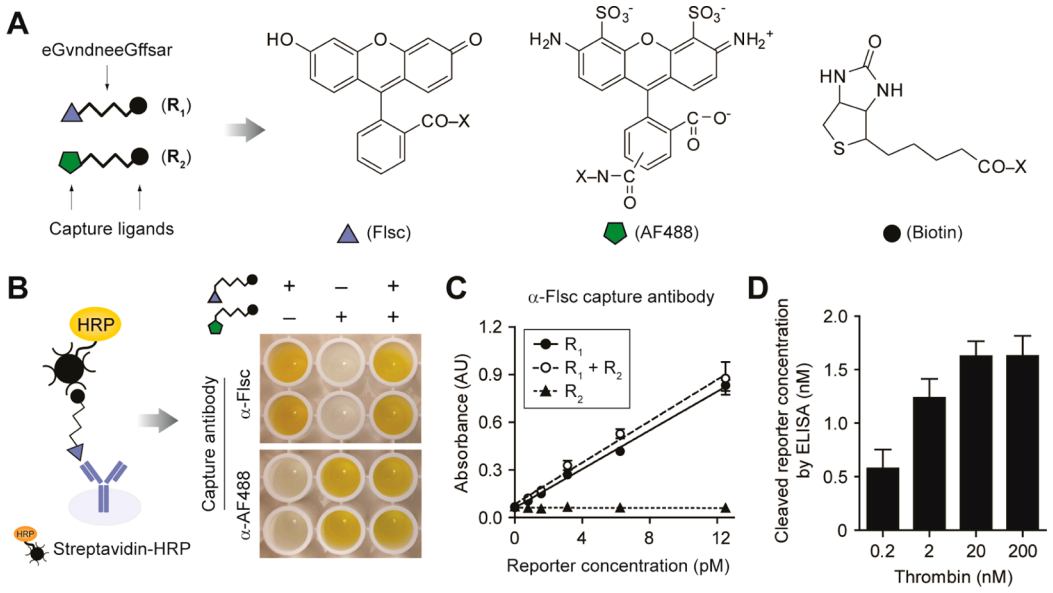

Figure 2. Designing ligand-encoded reporters for detection by ELISA. (A) Schematic of ligand-encoded reporters R_1 and R_2 along with chemical structures of associated ligands. (B) Schematic of ELISA sandwich complex and photograph of developed 96-well plates showing specific detection of R_1 and R_2 spiked into control urine samples. (C) Absorbance values (λ = 450 nm) of wells coated with anti-FIsc antibodies used to detect serial dilutions of R_1, $R_1 + R_2$, and R_2 in urine (n = 3 per condition, s.d.). (D) Quantification of the level of cleaved reporters (R_1) released from NWs after incubation with increasing concentrations of thrombin (n = 3 per dose, s.d.).

Supporting Information) sufficient to reduce fluorescence by over 90% *via* homoquenching (Figure S1C, Supporting Information) and then incubated the NWs (200 nM by peptide, 5 nM by NW) with purified thrombin (2 μM) or a panel of blood clotting proteases (FXa (160 nM), APC (60 nM), FIXa (90 nM), FVIIa (10 nM), FXIa (31 nM)), each present at its maximal physiological concentration (Figure 1B). Freely emitting peptide fragments that were released by thrombin activity rapidly increased sample fluorescence (red, Figure 1C). By contrast, negligible proteolysis was observed from the panel of noncognate proteases, as well as by thrombin in the presence of bivalirudin (Bival), a clinically approved direct thrombin inhibitor. To further investigate the ability to sense thrombin activity from blood, we spiked NWs into human plasma samples inactivated with sodium citrate (an anticoagulant that chelates the cofactor calcium) and monitored plasma fluorescence after the addition of excess calcium chloride ($CaCl_2$) to trigger coagulation, or phosphate buffered saline (PBS) as a control. Aligned with our previous observations with purified enzymes, plasma fluorescence markedly increased upon activation of the clotting cascade but not in control samples or in the presence of bivalirudin (Figure 1D). To test stability, we incubated fluorogenic NWs in 10% serum at 37 °C overnight and did not detect any significant differences in size (Figure S1D, Supporting Information) that would indicate precipitation or increases in sample fluorescence (Figure S1E, Supporting Information) that would indicate nonspecific substrate cleavage. Collectively, these results established the ability of our NWs to specifically sense the proteolytic activity of thrombin within the complex milieu of plasma, consistent with previously described thrombin-specific fluorogenic probes.[22]

Detection of Ligand-Encoded Reporters by ELISA. We next set out to build a system of ligand-encoded reporters that would allow quantification of protease activity in a 96-well format by ELISA, the primary detection platform for many clinical tests. Conventional ELISAs detect a target analyte *via* a sandwich complex composed of two affinity agents that bind to distinct epitopes on the analyte (Figure 2A). To build a synthetic reporter, we modified the protease-resistant peptide Glutamate-Fibrinopeptide B (Glu-fib, sequence = eGvndneeGffsar, lower case = D-isomer), which we selected for its high renal clearance efficiency,[35] at the termini with structurally distinct ligands (*i.e.*, FIsc or AF488) and biotin (labeled R_1 and R_2 respectively; Figure 2A). To test the immunoassay, these reporters were then spiked into urine and applied to 96-well plates precoated with capture antibodies (α-FIsc or α-AF488) before the presence of R_1 or R_2 was detected by the addition of neutravidin-horseradish peroxidase (HRP) and its catalytic development of 3,3′,5,5′-tetramethylbenzidine (TMB). As predicted from the specificities of the antibodies, a significant change in color appeared only in wells containing matched antibody-ligand pairs (+/− or −/+ wells, Figure 2B) and was not affected by the presence of noncognate reporters (+/+ wells). Identical trends were observed at the limits of detection for both capture antibodies (~3 pM, Figure 2C, Figure S3, Supporting Information), indicating

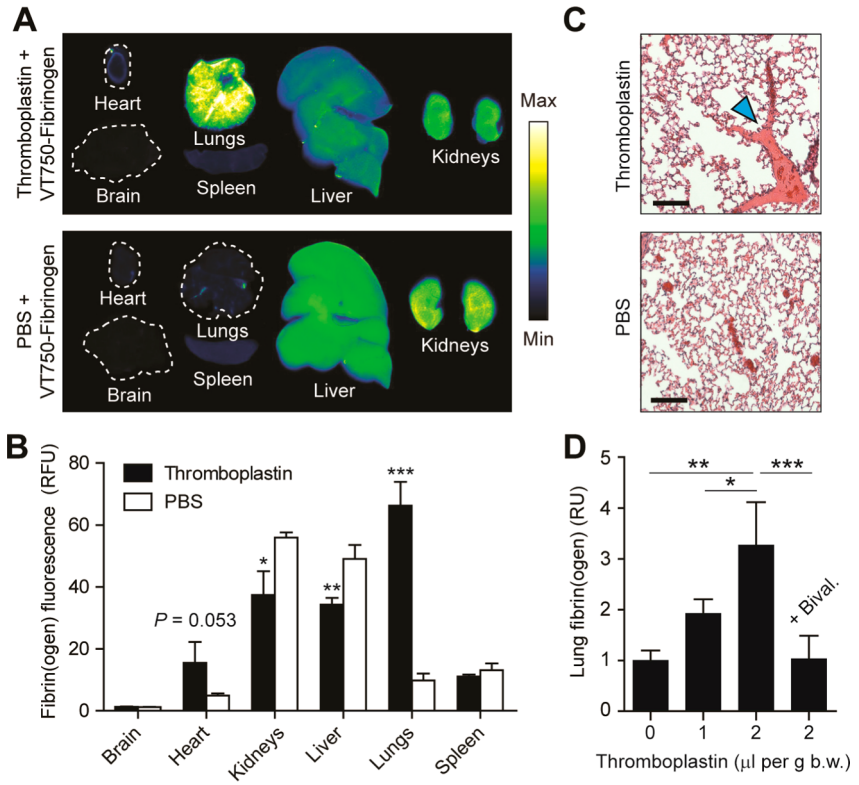

Figure 3. Induction of thrombosis by thromboplastin. (A) Near-infrared fluorescent scans of excised organs to monitor the deposition of VT750-labeled fibrinogen following intravenous administration of thromboplastin (2 μL/g of body weight) or PBS. (B) Quantification of the level of VT750-fibrin(ogen) deposited in organs harvested from thrombosis and control mice (*P < 0.05, **P < 0.01, ***P < 0.005, Student's t-test; n = 3 per group, s.d.). (C) Hematoxylin and eosin staining of lungs harvested from thrombosis and healthy mice (scale bar = 100 μm). Blue arrow denotes fibrin clot. (D) Quantification of fibrin deposited in the lungs in response to escalating doses of thromboplastin. Bival, bivalirudin (*P < 0.05, **P < 0.01, ***P < 0.005, one-way ANOVA with Tukey post-test; n = 3−5 mice, s.e.).

that our synthetic reporters were detected with high specificity and sensitivity comparable with protein-based ELISAs.[36] With an optimized thrombin substrate and a reporter system in place, we then incubated NWs (100 nM by peptide, 2.5 nM by NW) decorated with our final tandem peptide construct (sequence = biotin-eGvndneeGffsar(K-Flsc)GGfPRSGGGC, Figure S2B, Supporting Information) with increasing levels of thrombin and found that the amount of cleavage products released into solution (isolated by size filtration) was dose dependent, reaching a plateau likely due to cleavage of all available substrates and establishing our ability to monitor thrombin activity by ELISA (Figure 2D). Collectively, these results indicate that the specificity of ligand−antibody interactions can be used to build panels of orthogonal reporters for monitoring protease activity by standardized 96-well assays.

Characterization of Thromboplastin-Induced Pulmonary Embolism. We next investigated the ability of our synthetic biomarkers to detect thrombosis in living mice induced *via* intravenous (i.v.) administration of thromboplastin. This model has been used in the hematology literature to explore the role different vascular receptors play in host susceptibility to thrombosis and to probe the efficacy of new antithrombotic agents.[37−39] Thromboplastin triggers the clotting cascade through the extrinsic pathway *via* complexation of tissue factor and factor VII, and blood clots embolize to the lungs in this model, recapitulating the life-threatening clinical condition of pulmonary embolism (PE). To quantify PE formation, we coinjected mice with thromboplastin and the clot precursor fibrinogen labeled with the near-infrared fluorophore VT750 so that the formation of fibrin clots by thrombin-mediated proteolysis of fibrinogen could be quantified by fluorescent analysis of whole organs (Figure 3A). Within 30 min of administration, we observed a more than 6-fold increase in the level of fibrin(ogen) deposited within the lungs and significant decreases in the kidneys and liver (P < 0.005 by Student's t-test, n = 3 mice; Figure 3B), consistent with venous blood flow patterns that transport thrombi formed upon i.v. administration directly to the lungs from the heart, leading to depletion of VT750-fibrinogen in the other organs. Histochemical analysis of tissue sections corroborated these findings by revealing the presence of blood clots in lung sections (blue arrow, Figure 3C) that were absent in the other major organs (brain, heart, kidney, liver and spleen; Figure S4, Supporting Information) and in control animals. Animals given escalating but sublethal doses (observed

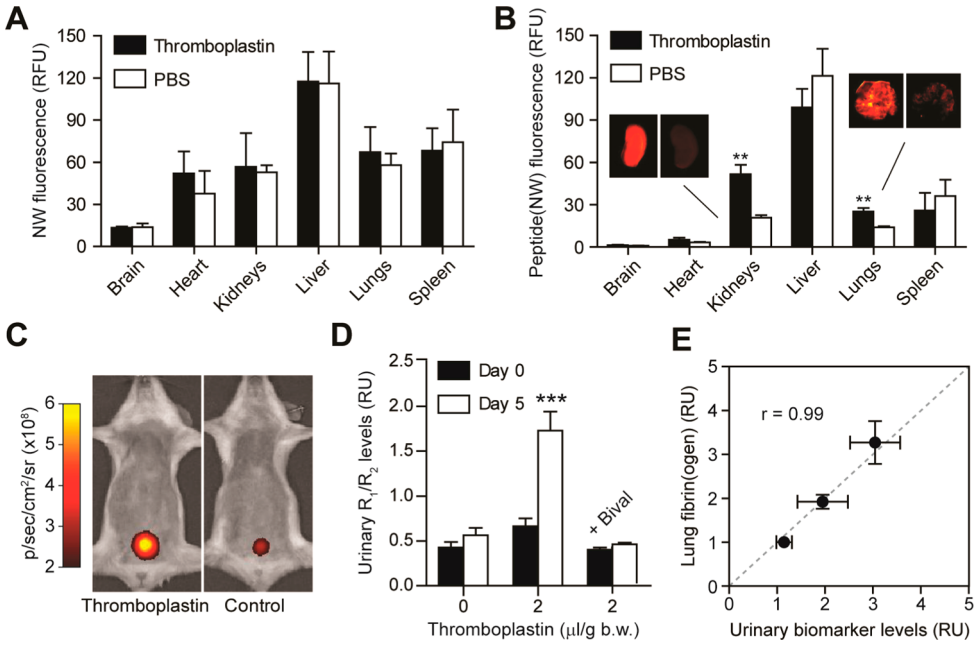

Figure 4. Noninvasive urinary detection of pulmonary embolism (A) Quantification of the distribution of VT750-labeled NWs in organs excised from mice treated with thromboplastin or PBS ($n = 3$ mice, s.d.). (B) Quantification of the fluorescent signal of organs after mice were infused mixtures of NWs conjugated with quenched substrates (labeled with VT750) and thromboplastin or PBS ($P < 0.01$, Student's t-test; $n = 3$ mice, s.d.). Inset shows representative fluorescent scans of the kidneys and the lungs. (C) *In vivo* fluorescent image after administration of NWs showing increased fluorescent signal localized to the bladders of mice challenged with thromboplastin. (D) Normalized urinary reporter levels (R_1/R_2) from healthy mice (day 0) and in response to thromboplastin and bivalirudin (day 5). Bival, bivalirudin (***$P < 0.005$, two-way ANOVA with Bonferroni post-test; $n = 5$ mice, s.e.). (E) Correlation plot of the clot burden in the lungs *versus* urinary biomarker levels (Pearson's $r = 0.999$; $n = 5-10$ mice, s.e.).**

LD50 ~ 3 μL per g b.w.) of thromboplastin accumulated fibrin(ogen) in the lungs in proportion to the dosage, and PEs were readily prevented in animals pretreated with bivalirudin ($P < 0.005$ by one-way ANOVA with Tukey post-test, $n = 3-5$ mice; Figure 3D, Figure S5, Supporting Information), confirming that clot formation is largely driven by the activity of thrombin. Altogether, these results established our ability to precisely control total clot burden in a model that resembles the clinical pathology of venous thrombosis.[38,40]

Detection of Pulmonary Embolism from Urine. Next, we characterized the pharmacokinetics of our synthetic biomarkers in the context of thrombosis. We injected mixtures of VT750-labeled NWs and thromboplastin into mice and observed no significant differences in NW distribution between the thromboplastin and control groups in all of the excised organs, including the lungs, indicating that thrombosis did not alter the biodistribution of the NW scaffold ($P > 0.05$ by Student's t-test, $n = 3$ mice; Figure 4A, Figure S6, Supporting Information). To monitor peptide cleavage and trafficking of the cleaved fragments, we coadministered NWs conjugated with fluorescently quenched substrates and observed significant increases in fluorescence in the lungs and kidneys by ~1.8 and ~2.5 fold over healthy animals, respectively ($P < 0.01$ by Student's t-test, $n = 3$ mice; Figure 4B, Figure S7, Supporting Information). Paired with our earlier observations showing that thromboplastin did not alter the biodistribution of the NWs and induced blood clots that were localized to the lung (*i.e.*, clots were not found in the kidneys), this finding provided evidence of peptide cleavage in the lungs and kidney accumulation of freely emitting fluorescent fragments. Immunofluorescent staining of lung sections further showed NW (green) localization with fibrin (red) at the sites of coagulation, which was absent in control sections (Figure S8, Supporting Information), supporting our hypothesis that circulating NWs can access local thrombi. To visualize the clearance efficiencies of the peptide fragments, we monitored mice by *in vivo* fluorescence imaging and observed a strong increase in fluorescent signal that was localized to the bladder of thrombotic mice relative to controls (Figure 4C). Taken together, our data illustrated that our synthetic biomarkers can systemically survey the vasculature for thrombin activity and release reporters at sites of thrombosis, which are then cleared efficiently into the host urine.

In considering clinical translation, we sought to develop a method to account for variations in the production rate of urine expected in individuals that could affect the urine concentration of our reporters. Urinary production rates are mainly dependent on the hydration state of the host (ranging from 50–1200 mOsm/kg of H_2O in humans)[41] and affected by many external factors (*e.g.*, circadian rhythm, diet, activity, and others).

Approaches to determine the concentration of urine include measuring the level of creatinine,[42,43] a byproduct of muscle metabolism that filters into the urine at a steady state when at rest, or i.v. administration of inulin,[44−46] a polysaccharide that is not actively absorbed or secreted by the kidneys and whose appearance in urine is directly related to the rate of urine production. Motivated by the clinical precedent set by inulin, we hypothesized that because our free reporters (R_1, R_2) are built from Glu-fib, which is likewise biologically inert,[35] their filtration into urine following i.v. administration would be indicative of the concentration of urine. To test this, we excessively hydrated a cohort of mice with a subcutaneous bolus of saline equivalent to 10% of their body weight followed by i.v. administration of free R_2. Compared to control mice infused with R_2 only, hydrated mice produced over 2.5 fold more urine within 2 h ($P < 0.005$ by Student's *t*-test, Figure S9A, Supporting Information) and their urinary concentration of R_2 decreased by ∼50% ($P < 0.005$ by Student's *t*-test, Figure S9B, Supporting Information), showing that our free reporters could be used to monitor the hydration state and urine concentration of the animals. We next sought to monitor thromboplastin-induced PEs by urine analysis of the response of our synthetic biomarkers to thrombin activity. To simulate serial monitoring that frequently occurs in inpatient settings, we first determined the basal activity in healthy cohorts of animals each receiving thrombin-sensitive NWs and a free reporter (R_2) for urine normalization (Figure 4D). After five days to allow NWs to fully clear (half-life ∼6 h),[17] we administered a mixture of thromboplastin, NWs, and R_2 into the same mice and quantified reporter levels by ELISA. When compared to their healthy state (day 0), the induction of PEs (day 5) resulted in significant elevations in the level of urinary cleavage fragments by up to 3-fold ($P < 0.005$ by two-way ANOVA with Bonferroni post-test, $n = 5$ mice; Figure 4D). In mice treated with bivalirudin prior to thrombotic challenge (dose = 2 μL per g of b.w.), reporter levels were abrogated, consistent with our earlier findings showing the ability of bivalirudin to inhibit thrombin activity and prevent the formation of PEs. When the urinary biomarker marker levels from thromboplastin-challenged mice were directly compared to the amount of fibrin(ogen) deposited at identical doses of thromboplastin (Figure 3D), we found a striking correlation to the disease burden with a correlation coefficient of 0.99 (Pearson's *r*, Figure 4E). Collectively, our findings showed that synthetic biomarkers can monitor thrombin activity in living mice and quantitatively measure the aggregate burden of sublethal PEs from the urine by ELISA.

CONCLUSION

By harnessing the capacity of peptide-decorated NWs to circulate and sense their local vascular microenvironment, we have engineered synthetic biomarkers that can detect thrombin activity *in vivo* and noninvasively quantify the aggregate amount of active clots. Unlike other nanoparticle sensors that function by producing a localized signal,[21−24,47−49] our NWs sense protease activity by releasing reporters locally at the sites of thrombus formation but are then filtered and detected remotely from the urine. Interestingly, in imaging studies using fluorogenic thrombin-cleavable probes, this "washout" of the cleaved fragments was also directly observed by monitoring the attenuation of the strength of the detection signal localized at the thrombi.[21] Similar to circulating biomarkers, our approach can reveal thrombosis at sites deep within the body, such as the lungs, that are difficult to detect with fluorogenic probes because of tissue absorption and scattering of light.[50] This property allows urine analysis to integrate and quantitatively assess the burden of vascular clots, which would otherwise require systemic exploration by imaging. In addition, we developed a panel of heterobifunctional reporters that can be detected by standardized 96-well plate assays, removing the need for mass spectrometry as described in our previous study.[17] This reporter system is readily extensible by incorporating additional ligand-capture agent pairs and is amenable for detection by other methods including paper-based tests at the point of care.[51−53] Potential improvements to this platform include the use of new thrombin-sensitive substrates that are significantly more specific to reduce background activities from other plasma proteases,[34,54] and further functionalizing NWs, which are superparamagnetic,[30] with fibrin-targeted ligands to allow contrast-enhanced magnetic resonance imaging (MRI) of individual clots simultaneously with urine analysis.[55−57] To allow clinical translation, we chose to use NWs because we previously showed that they are well-tolerated by mice, and similar FDA-approved formulations of iron oxide nanoparticles (*e.g.*, Ferridex) are already used in patients;[17,58−63] however, thrombin substrates may also be attached to other long-circulating nanoparticles, such as dextran or liposomes, to prevent peptide filtration into urine until cleavage by proteases.

Looking forward, several clinical applications warrant further investigation with this approach. Because sensing thrombin activity requires NWs to access the sites of coagulation, the local architecture of the vessels, clotting kinetics of the thrombi, and degree of occlusion would all likely influence the rate of peptide cleavage and clearance efficiencies of the reporters.[21,23,24] Therefore, additional studies that utilize specific clinical models, such as deep vein thrombosis (DVT), would be important to determine the type of clots this approach could be used to detect. Further, whereas MRI or ultrasound can resolve anatomical features of clots, they cannot discriminate stable from extending thrombi without serial imaging.

Related studies in atherosclerosis showed that thrombin activity could be used to differentiate stable from severe plaques, highlighting the potential benefits of an activity-based measurement compared to imaging alone.[23] In summary, we believe this work further broadens the repertoire of nanomedicines that could be used for noninvasive monitoring of disease, and we anticipate generalization to additional clinical settings in which dysregulated thrombin activity is prominent.

MATERIALS AND METHODS

Peptide Nanoworm Synthesis. Aminated iron oxide NWs were synthesized according to previously published protocols.[30] Peptides (biotin-eGvndneeGffsar(K-Flsc)GGfPRSGGGC, lower case = D-isomer) were synthesized by the Tufts University Core Facility peptide synthesis service. To conjugate peptides to NWs, NWs were first reacted with succinimidyl iodoacetate (Pierce) to introduce sulfhydryl-reactive handles. Cysteine terminated peptides and 20 kDa polyethylene glycol−SH (Laysan Bio.) were then mixed with NWs (95:20:1 molar ratio) for one hour at room temperature (RT) and purified by fast protein liquid chromatography. Stock solutions were stored in PBS at 4 °C. The number of fluorescein-labeled peptides per NWs was determined by absorbance spectroscopy using the absorbance of fluorescein (490 nm) and its extinction coefficient (78 000 cm^{-1} M^{-1}). For pharmacokinetic studies, NWs were first reacted with NHS-VT750 (PerkinElmer) prior to PEGylation as above. For fluorogenic assays, thrombin substrates were synthesized with a terminal fluorescein or VT750 in lieu of a reporter.

***In Vitro* Stability Assays.** NWs (1 μM by peptide, 25 nM by NW) were incubated in 10% fetal bovine serum at 37 °C. At selected time points, the particle size was measured by dynamic light scattering (Malverin Zetasizer Nano Series) and the fluorescence intensity was measured by microplate reader (SpectroMax Gemini EM).

***In Vitro* Protease Assays.** NWs (200 nM by peptide, 5 nM by NW) were mixed with human thrombin (2 μM), FVIIa (10 nM), FIXa (90 nM), FXa (160 nM), FXIa (31 nM), and activated protein C (60 nM), all purchased from Haematologic Technologies, in a 384-well plate at 37 °C in activity buffers according to the manufacturer's instructions and monitored with a microplate reader (SpectroMax Gemini EM). For plasma studies, NWs were mixed with 50 μL of control human plasma (Thermo Scientific) and 50 μL of 80 mM $CaCl_2$ (Sigma) or PBS. For thrombin inhibition experiments, bivalirudin (Anaspec) was added to a final concentration of 5 mg/mL and preincubated for 2 min prior to addition of NWs. For the ELISA studies, NWs (100 nM by peptide, 2.5 nM by NW) were incubated with thrombin for 10 min at 37 °C, and cleaved reporters (R_1) were purified from NWs by centrifugal size filtration (3 kDa MWCO).

ELISA Detection of Bifunctionalized Reporters. The bottom of 96-well plates (Thermo Scientific) were coated with either 0.8 μg/mL of anti-Flsc (GeneTex, GTX19224) or 0.4 μg/mL of anti-Alex Fluor 488 (Invitrogen, A11094) diluted in PBS overnight at 4 °C. Plates were blocked with 1% w/v bovine serum albumin (Sigma) in PBS for 1 h before 100 μL of samples were added. Reporters captured on the plate were then detected by adding 100 μL of 0.2 μg/mL neutravidin-HRP (Pierce), developed with 50 μL TMB solution (Thermo Scientific) for 5−15 min, and quenched with 50 μL of HCl before the absorbance of the wells was determined by microplate analysis (SpectraMax Plus, Molecular Devices) at 450 nm. Plates were washed 3× with PBST between each step, and incubation occurred at RT unless otherwise stated.

Characterization of Thromboplastin-Induced Thrombosis. Each vial of thromboplastin containing 3−4 mg (from rabbit brain, Sigma) was dissolved in 2 mL of PBS. To quantify fibrin deposition, bovine fibrinogen (Sigma) was reacted with 3-fold molar excess of VT750 for 1 h at RT and purified by centrifugal size filtration (100 kDa MWCO, Millipore). Swiss Webster mice (Taconic) were lightly anesthetized with isofluorane and administered mixtures of VT750-fibrinogen (1 nmol by VT750) with thromboplastin (n = 3 mice per dose) *via* tail vein injections. After 30 min, mice were euthanized by CO_2 asphyxiation, and organs were scanned on the LI-COR Odyssey Infrared Imaging System. Fluorescence in each organ was quantified using Image J software (NIH). To test thrombin inhibition, mice were intravenously administered bivalirudin (10 mg/kg) 5 min prior to coinjection of thromboplastin. For histology, lungs were inflated with 4% paraformaldehyde, while all other organs were incubated in 4% paraformaldehyde for 1−2 h at RT. All organs were stored in 70% ethanol until paraffin-embedding, sectioning, and staining (Koch Institute Histology Core).

NW Pharmacokinetics. To analyze NW and peptide pharmacokinetics, mice were given either VT750-labeled NWs (5 μM by VT750) or NWs conjugated with VT750-labeled peptides (600 nM by peptide, 15 nM by NW) in conjunction with thromboplastin. To analyze tissue sections by immunostaining, NWs (600 nM by peptide, 15 nM by NW) and thromboplastin (2 μL/g of b.w.) were administered to mice, and major organs were harvested after 30 min. Representative lung sections were stained for NWs (anti-Flsc primary, Invitrogen, A11090), fibrin (Nordic, GAM/Fbg/Bio) and Hoechst (Invitrogen, H3569) before analysis by fluorescence microscopy (Nikon Eclipse Ti).

Effect of Hydration State on Urine Concentration. The free reporter R_2 (biotin-eGvndneeGffsar(K-AF488)) was synthesized by the Tufts University Core Facility peptide synthesis service. Mice (n = 5 mice) were anesthetized and injected subcutaneously with a PBS bolus equivalent to 10% of their body weights. After two hours, R_2 (125 nm) was administered to mice *via* a tail vein injection. Mice were placed over 96-well plates surrounded by cylindrical sleeves for 30 min post-NW injection to allow mice to void. Urine samples were stored at −80 °C until ELISA analysis.

Urinary Monitoring of Thrombosis. Experiments were conducted in a paired setup. Thrombin-sensitive NWs (600 nM by peptide, 15 nM by NW) and R_2 (125 nM) were coinjected into healthy mice (n = 5−10 mice) to determine background protease activity and placed over 96-well plates to collect urine. Five days later, mice were again dosed with NWs, R_2, and thromboplastin before urine was collected from mice 30 min post-NW injection. For thrombin inhibition experiments, mice were intravenously administered bivalirudin (10 mg/kg) 5 min prior to NW/R_2 injections. Urine samples were stored at −80 °C until ELISA analysis.

Statistical Analyses. ANOVA analyses and Student's t-test were calculated with GraphPad 5.0 (Prism). Pearson's r coefficient was calculated with Excel (Microsoft Office).

All animal work was approved by the committee on animal care (MIT, protocol #0411-036-14).

Conflict of Interest: The authors declare no competing financial interest.

Acknowledgment. We thank the Swanson Biotechnology Center (MIT) for use of their animal imaging facilities and assistance with tissue sectioning. We thank Dr. Heather Fleming (MIT) for critical readings of the manuscript. This work is supported by a grant from the Koch Institute Frontier Research Program through the Koch Institute Frontier Research Fund and the Kathy and Curt Marble Cancer Research Fund, the Mazumdar-Shaw International Oncology Fellows Program, and the MIT Deshpande Center Innovation Grant. K.Y.L. acknowledges support from CCNE (5 U54 CA151884-03). Dr. G.A.K. acknowledges support from the Ruth L. Kirschstein National Research Service Award (F32CA159496-02) and holds a Career Award at the Scientific Interface from the Burroughs Wellcome Fund. Dr. S. N.B is an HHMI Investigator. The authors wish to dedicate this paper to the memory of Officer Sean Collier, for his caring service to the MIT community and for his sacrifice.

Supporting Information Available: Supplementary figures. This material is available free of charge *via* the Internet at http://pubs.acs.org.

REFERENCES AND NOTES

1. Pisitkun, T.; Johnstone, R.; Knepper, M. A. Discovery of Urinary Biomarkers. *Mol. Cell. Proteomics* **2006**, *5*, 1760–1771.
2. Barratt, J.; Topham, P. Urine Proteomics: The Present and Future of Measuring Urinary Protein Components in Disease. *Can. Med. Assoc. J.* **2007**, *177*, 361–368.
3. Adachi, J.; Kumar, C.; Zhang, Y.; Olsen, J. V.; Mann, M. The Human Urinary Proteome Contains More than 1500 Proteins, Including a Large Proportion of Membrane Proteins. *Genome Biol.* **2006**, *7*, R80.
4. Wide, L.; Gemzell, C. A. An Immunological Pregnancy Test. *Acta Endrocrinol.* **1960**, *XXXV*, 261–267.
5. Cole, L. A.; Kardana, A.; Seifer, D. B.; Bohler, H. C. Urine hCG Beta-Subunit Core Fragment, a Sensitive Test for Ectopic Pregnancy. *J. Clin. Endocrinol. Metab.* **1994**, *78*, 497–499.
6. Hinokio, Y.; Suzuki, S.; Hirai, M.; Chiba, M.; Hirai, A.; Toyota, T. Oxidative DNA Damage in Diabetes Mellitus: Its Association with Diabetic Complications. *Diabetologia* **1999**, *42*, 995–998.
7. Nishikawa, T.; Sasahara, T.; Kiritoshi, S.; Sonoda, K.; Senokuchi, T.; Matsuo, T.; Kukidome, D.; Wake, N.; Matsumura, T.; Miyamura, N.; *et al.* Evaluation of Urinary 8-Hydroxydeoxy-Guanosine as a Novel Biomarker of Macrovascular Complications in Type 2 Diabetes. *Diabetes Care* **2003**, *26*, 1507–1512.
8. Wu, L. L.; Chiou, C. C.; Chang, P. Y.; Wu, J. T. Urinary 8-OHdG: A Marker of Oxidative Stress to DNA and a Risk Factor for Cancer, Atherosclerosis and Diabetics. *Clin. Chim. Acta* **2004**, *339*, 1–9.
9. Rossing, K.; Mischak, H.; Dakna, M.; Zürbig, P.; Novak, J.; Julian, B. A.; Good, D. M.; Coon, J. J.; Tarnow, L.; Rossing, P. Urinary Proteomics in Diabetes and CKD. *J. Am. Soc. Nephrol.* **2008**, *19*, 1283–1290.
10. Tesch, G. H. Review: Serum and Urine Biomarkers of Kidney Disease: A Pathophysiological Perspective. *Nephrology* **2010**, *15*, 609–616.
11. Fassett, R. G.; Venuthurupalli, S. K.; Gobe, G. C.; Coombes, J. S.; Cooper, M. A.; Hoy, W. E. Biomarkers in Chronic Kidney Disease: A Review. *Kidney Int.* **2011**, *80*, 806–821.
12. Mishra, J.; Ma, Q.; Prada, A.; Mitsnefes, M.; Zahedi, K.; Yang, J.; Barasch, J.; Devarajan, P. Identification of Neutrophil Gelatinase-Associated Lipocalin as a Novel Early Urinary Biomarker for Ischemic Renal Injury. *J. Am. Soc. Nephrol.* **2003**, *14*, 2534–2543.
13. Isomaa, B.; Almgren, P.; Tuomi, T.; Forsén, B.; Lahti, K.; Nissén, M.; Taskinen, M.-R.; Groop, L. Cardiovascular Morbidity and Mortality Associated With the Metabolic Syndrome. *Diabetes Care* **2001**, *24*, 683–689.
14. Palaniappan, L.; Carnethon, M.; Fortmann, S. P. Association Between Microalbuminuria and the Metabolic Syndrome: NHANES III. *Am. J. Hypertens.* **2003**, *16*, 952–958.
15. Moses, M. A.; Wiederschain, D.; Loughlin, K. R.; Zurakowski, D.; Lamb, C. C.; Freeman, M. R. Increased Incidence of Matrix Metalloproteinases in Urine of Cancer Patients. *Cancer Res.* **1998**, *58*, 1395–1399.
16. Roy, R.; Yang, J.; Moses, M. A. Matrix Metalloproteinases As Novel Biomarkers and Potential Therapeutic Targets in Human Cancer. *J. Clin. Oncol.* **2009**, *27*, 5287–5297.
17. Kwong, G. A.; von Maltzahn, G.; Murugappan, G.; Abudayyeh, O.; Mo, S.; Papayannopoulos, I. A.; Sverdlov, D. Y.; Liu, S. B.; Warren, A. D.; Popov, Y.; *et al.* Mass-Encoded Synthetic Biomarkers for Multiplexed Urinary Monitoring of Disease. *Nat. Biotechnol.* **2013**, *31*, 63–70.
18. Robbins, S. L.; Kumar, V.; Cotran, R. S. *Robbins and Cotran Pathologic Basis of Disease*; Saunders/Elsevier: Philadelphia, 2010.
19. Davie, E. W.; Kulman, J. D. An Overview of the Structure and Function of Thrombin. *Semin. Thromb. Hemostasis* **2006**, *32*, 003–015.
20. Huntington, J. A. Molecular Recognition Mechanisms of Thrombin. *Semin. Thromb. Hemostasis* **2005**, *3*, 1861–1872.
21. Jaffer, F. A.; Tung, C.-H.; Gerszten, R. E.; Weissleder, R. *In Vivo* Imaging of Thrombin Activity in Experimental Thrombi With Thrombin-Sensitive Near-Infrared Molecular Probe. *Arterioscler., Thromb., Vasc. Biol.* **2002**, *22*, 1929–1935.
22. Tung, C.-H.; Gerszten, R. E.; Jaffer, F. A.; Weissleder, R. A Novel Near-Infrared Fluorescence Sensor for Detection of Thrombin Activation in Blood. *ChemBioChem* **2002**, *3*, 207–211.
23. Olson, E. S.; Whitney, M. A.; Friedman, B.; Aguilera, T. A.; Crisp, J. L.; Baik, F. M.; Jiang, T.; Baird, S. M.; Tsimikas, S.; Tsien, R. Y.; *et al. In Vivo* Fluorescence Imaging of Atherosclerotic Plaques with Activatable Cell-Penetrating Peptides Targeting Thrombin Activity. *Integr. Biol.* **2012**, *4*, 595–605.
24. Whitney, M.; Savariar, E. N.; Friedman, B.; Levin, R. A.; Crisp, J. L.; Glasgow, H. L.; Lefkowitz, R.; Adams, S. R.; Steinbach, P.; Nashi, N.; *et al.* Ratiometric Activatable Cell-Penetrating Peptides Provide Rapid *in Vivo* Readout of Thrombin Activation. *Angew. Chem., Int. Ed.* **2013**, *52*, 325–330.
25. Bounameaux, H.; de Moerloose, P.; Perrier, A.; Reber, G. Plasma Measurement of D-Dimer as Diagnostic Aid in Suspected Venous Thromboembolism: An Overview. *Thromb. Haemostasis* **1994**, *71*, 1–6.
26. Ginsberg, J. S.; Wells, P. S.; Kearon, C.; Anderson, D.; Crowther, M.; Weitz, J. I.; Bormanis, J.; Brill-Edwards, P.; Turpie, A. G.; MacKinnon, B.; *et al.* Sensitivity and Specificity of a Rapid Whole-Blood Assay for D-Dimer in the Diagnosis of Pulmonary Embolism. *Ann. Intern. Med.* **1998**, *129*, 1006–1011.
27. Becker, R. C.; Spencer, F. A. Thrombin: Structure, Biochemistry, Measurement, and Status in Clinical Medicine. *J. Thromb. Thrombolysis* **1998**, *5*, 215–229.
28. Choi, H. S.; Liu, W.; Misra, P.; Tanaka, E.; Zimmer, J. P.; Itty Ipe, B.; Bawendi, M. G.; Frangioni, J. V. Renal Clearance of Quantum Dots. *Nat. Biotechnol.* **2007**, *25*, 1165–1170.
29. Park, J.-H.; Maltzahn, G. v.; Zhang, L.; Schwartz, M. P.; Ruoslahti, E.; Bhatia, S. N.; Sailor, M. J. Magnetic Iron Oxide Nanoworms for Tumor Targeting and Imaging. *Adv. Mater.* **2008**, *20*, 1630–1635.
30. Park, J.-H.; von Maltzahn, G.; Zhang, L.; Derfus, A. M.; Simberg, D.; Harris, T. J.; Ruoslahti, E.; Bhatia, S. N.; Sailor, M. J. Systematic Surface Engineering of Magnetic Nanoworms for *in Vivo* Tumor Targeting. *Small* **2009**, *5*, 694–700.
31. Mitchell, G. A.; Gargiulo, R. J.; Huseby, R. M.; Lawson, D. E.; Pochron, S. P.; Sehuanes, J. A. Assay for Plasma Heparin Using a Synthetic Peptide Substrate for Thrombin: Introduction of the Fluorophore Aminoisophthalic Acid, Dimethyl Ester. *Thromb. Res.* **1978**, *13*, 47–52.
32. Asai, K.; Asai, M. A Colorimetric Assay for Plasma Antithrombin III Using a New Synthetic Peptide Substrate (PS-915). *Clin. Chim. Acta* **1984**, *144*, 163–171.
33. Larsen, M. L.; Abildgaard, U.; Teien, A. N.; Gjesdal, K. Assay of Plasma Heparin Using Thrombin and the Chromogenic Substrate H-D-Phe-Pip-Arg-pNA (S-2238). *Thromb. Res.* **1978**, *13*, 285–288.
34. Rijkers, D. S.; Wielders, S. J. H.; Tesser, G. I.; Hemker, H. C. Design and Synthesis of Thrombin Substrates with Modified Kinetic Parameters. *Thromb. Res.* **1995**, *79*, 491–499.
35. Morris, T. A.; Marsh, J. J.; Burrows, C. M.; Chiles, P. G.; Konopka, R. G.; Pedersen, C. A. Urine and Plasma Levels of Fibrinopeptide B in Patients with Deep Vein Thrombosis and Pulmonary Embolism. *Thromb. Res.* **2003**, *110*, 159–165.
36. Rosi, N. L.; Mirkin, C. A. Nanostructures in Biodiagnostics. *Chem. Rev.* **2005**, *105*, 1547–1562.
37. Weiss, E. J.; Hamilton, J. R.; Lease, K. E.; Coughlin, S. R. Protection Against Thrombosis in Mice Lacking PAR3. *Blood* **2002**, *100*, 3240–3244.
38. Lenain, N.; Freund, M.; Léon, C.; Cazenave, J. P.; Gachet, C. Inhibition of Localized Thrombosis in P2Y1-Deficient Mice and Rodents Treated with MRS2179, a P2Y1 Receptor

Antagonist. *Semin. Thromb. Hemostasis* **2003**, *1*, 1144–1149.
39. Smyth, S. S.; Reis, E. D.; Väänänen, H.; Zhang, W.; Coller, B. S. Variable Protection of β3-Integrin-Deficient Mice from Thrombosis Initiated by Different Mechanisms. *Blood* **2001**, *98*, 1055–1062.
40. Mackman, N. Triggers, Targets and Treatments for Thrombosis. *Nature* **2008**, *451*, 914–918.
41. Koeppen, B. M.; Stanton, B. A. *Renal Physiology*; Mosby Elsevier: Philadelphia, 2007.
42. Vestergaard, P.; Leverett, R. Constancy of Urinary Creatinine Excretion. *J. Lab. Clin. Med.* **1958**, *51*, 211–218.
43. Wyss, M.; Kaddurah-Daouk, R. Creatine and Creatinine Metabolism. *Physiol. Rev.* **2000**, *80*, 1107–1213.
44. Roe, J. H.; Epstein, J. H.; Goldstein, N. P. A Photometric Method for the Determination of Inulin in Plasma and Urine. *J. Biol. Chem.* **1949**, *178*, 839–845.
45. Gaspari, F.; Perico, N.; Remuzzi, G. Measurement of Glomerular Filtration Rate. *Kidney Int., Suppl.* **1997**, *63*, S151–S154.
46. Qi, Z.; Whitt, I.; Mehta, A.; Jin, J.; Zhao, M.; Harris, R. C.; Fogo, A. B.; Breyer, M. D. Serial Determination of Glomerular Filtration Rate in Conscious Mice Using FITC-Inulin Clearance. *Am. J. Physiol.:Renal, Fluid Electrolyte Physiol.* **2004**, *286*, F590–F596.
47. Ghadiali, J. E.; Stevens, M. M. Enzyme-Responsive Nanoparticle Systems. *Adv. Mater.* **2008**, *20*, 4359–4363.
48. Welser, K.; Adsley, R.; Moore, B. M.; Chan, W. C.; Aylott, J. W. Protease Sensing with Nanoparticle Based Platforms. *Analyst* **2011**, *136*, 29–41.
49. de la Rica, R.; Aili, D.; Stevens, M. M. Enzyme-Responsive Nanoparticles for Drug Release and Diagnostics. *Adv. Drug Delivery Rev.* **2012**, *64*, 967–978.
50. Frangioni, J. V. *In Vivo* Near-Infrared Fluorescence Imaging. *Curr. Opin. Chem. Biol.* **2003**, *7*, 626–634.
51. Yager, P.; Domingo, G. J.; Gerdes, J. Point-of-Care Diagnostics for Global Health. *Ann. Rev. Biomed. Eng.* **2008**, *10*, 107–144.
52. Martinez, A. W.; Phillips, S. T.; Whitesides, G. M.; Carrilho, E. Diagnostics for the Developing World: Microfluidic Paper-Based Analytical Devices. *Anal. Chem.* **2009**, *82*, 3–10.
53. Warren, A. D.; Kwong, G. A.; Wood, D. K.; Lin, K. Y.; Bhatia, S. N. Point-of-Care Diagnostics for Non-Communicable Diseases Using Synthetic Urinary Biomarkers and Paper Microfluidics. Unpublished work.
54. Backes, B. J.; Harris, J. L.; Leonetti, F.; Craik, C. S.; Ellman, J. A. Synthesis of Positional-scanning Libraries of Fluorogenic Peptide Substrates to Define the Extended Substrate Specificity of Plasmin and Thrombin. *Nat. Biotechnol.* **2000**, *18*, 187–193.
55. Botnar, R. M.; Perez, A. S.; Witte, S.; Wiethoff, A. J.; Laredo, J.; Hamilton, J.; Quist, W.; Parsons, E. C.; Vaidya, A.; Kolodziej, A.; *et al. In Vivo* Molecular Imaging of Acute and Subacute Thrombosis Using a Fibrin-Binding Magnetic Resonance Imaging Contrast Agent. *Circulation* **2004**, *109*, 2023–2029.
56. Simberg, D.; Duza, T.; Park, J. H.; Essler, M.; Pilch, J.; Zhang, L.; Derfus, A. M.; Yang, M.; Hoffman, R. M.; Bhatia, S.; *et al.* Biomimetic Amplification of Nanoparticle Homing to Tumors. *Proc. Natl. Acad. Sci. U. S. A.* **2007**, *104*, 932–936.
57. Hara, T.; Bhayana, B.; Thompson, B.; Kessinger, C. W.; Khatri, A.; McCarthy, J. R.; Weissleder, R.; Lin, C. P.; Tearney, G. J.; Jaffer, F. A. Molecular Imaging of Fibrin Deposition in Deep Vein Thrombosis Using Fibrin-targeted Near-Infrared Fluorescence. *J. Am. Coll. Cardiol.: Cardiovasc. Imaging* **2012**, *5*, 607–615.
58. Imai, Y.; Murakami, T.; Yoshida, S.; Nishikawa, M.; Ohsawa, M.; Tokunaga, K.; Murata, M.; Shibata, K.; Zushi, S.; Kurokawa, M.; *et al.* Superparamagnetic Iron Oxide-Enhanced Magnetic Resonance Images of Hepatocellular Carcinoma: Correlation with Histological Grading. *Hepatology* **2000**, *32*, 205–212.
59. Reimer, P.; Jähnke, N.; Fiebich, M.; Schima, W.; Deckers, F.; Marx, C.; Holzknecht, N.; Saini, S. Hepatic Lesion Detection and Characterization: Value of Nonenhanced MR Imaging, Superparamagnetic Iron Oxide-Enhanced MR Imaging, and Spiral CT-ROC Analysis. *Radiology* **2000**, *217*, 152–158.
60. Harisinghani, M. G.; Barentsz, J.; Hahn, P. F.; Deserno, W. M.; Tabatabaei, S.; van de Kaa, C. H.; de la Rosette, J.; Weissleder, R. Noninvasive Detection of Clinically Occult Lymph-Node Metastases in Prostate Cancer. *N. Engl. J. Med.* **2003**, *348*, 2491–2499.
61. Reimer, P.; Balzer, T. Ferucarbotran (Resovist): A New Clinically Approved RES-Specific Contrast Agent for Contrast-Enhanced MRI of the Liver: Properties, Clinical Development, and Applications. *Eur. Radiol.* **2003**, *13*, 1266–1276.
62. Tanimoto, A.; Kuribayashi, S. Application of Superparamagnetic Iron Oxide to Imaging of Hepatocellular Carcinoma. *Eur. J. Radiol.* **2006**, *58*, 200–216.
63. Heesakkers, R. A. M.; Jager, G. J.; Hövels, A. M.; de Hoop, B.; van den Bosch, H. C. M.; Raat, F.; Witjes, J. A.; Mulders, P. F. A.; van der Kaa, C. H.; Barentsz, J. O. Prostate Cancer: Detection of Lymph Node Metastases Outside the Routine Surgical Area with Ferumoxtran-10-Enhanced MR Imaging. *Radiology* **2009**, *251*, 408–414.

Supporting Information

Nanoparticles that Sense Thrombin Activity as Synthetic Urinary Biomarkers of Thrombosis

Kevin Y. Lin[1], Gabriel A. Kwong[2,3], Andrew D. Warren[2,3], David K. Wood[2,3,4], Sangeeta N. Bhatia[2,3,5,6,7,8]*

[1]Department of Chemical Engineering, Massachusetts Institute of Technology (MIT), Cambridge, MA 02139, United States; [2]Harvard-MIT Division of Heath Sciences and Technology, MIT, Cambridge, MA 02139, United States; [3]Institute for Medical Engineering and Science, MIT, Cambridge, MA 02139, United States; [4]Department of Biomedical Engineering, University of Minnesota, Minneapolis, MN 55455, United States; [5]Electrical Engineering and Computer Science, David H. Koch Institute for Integrative Cancer Research, MIT, Cambridge, MA 02139, United States; [6]Broad Institute of Harvard and MIT, Cambridge, MA 02139, United States; [7]Department of Medicine, Brigham and Women's Hospital, Boston, MA 02115, United States; [8]Howard Hughes Medical Institute, Cambridge, MA 02139, United States.

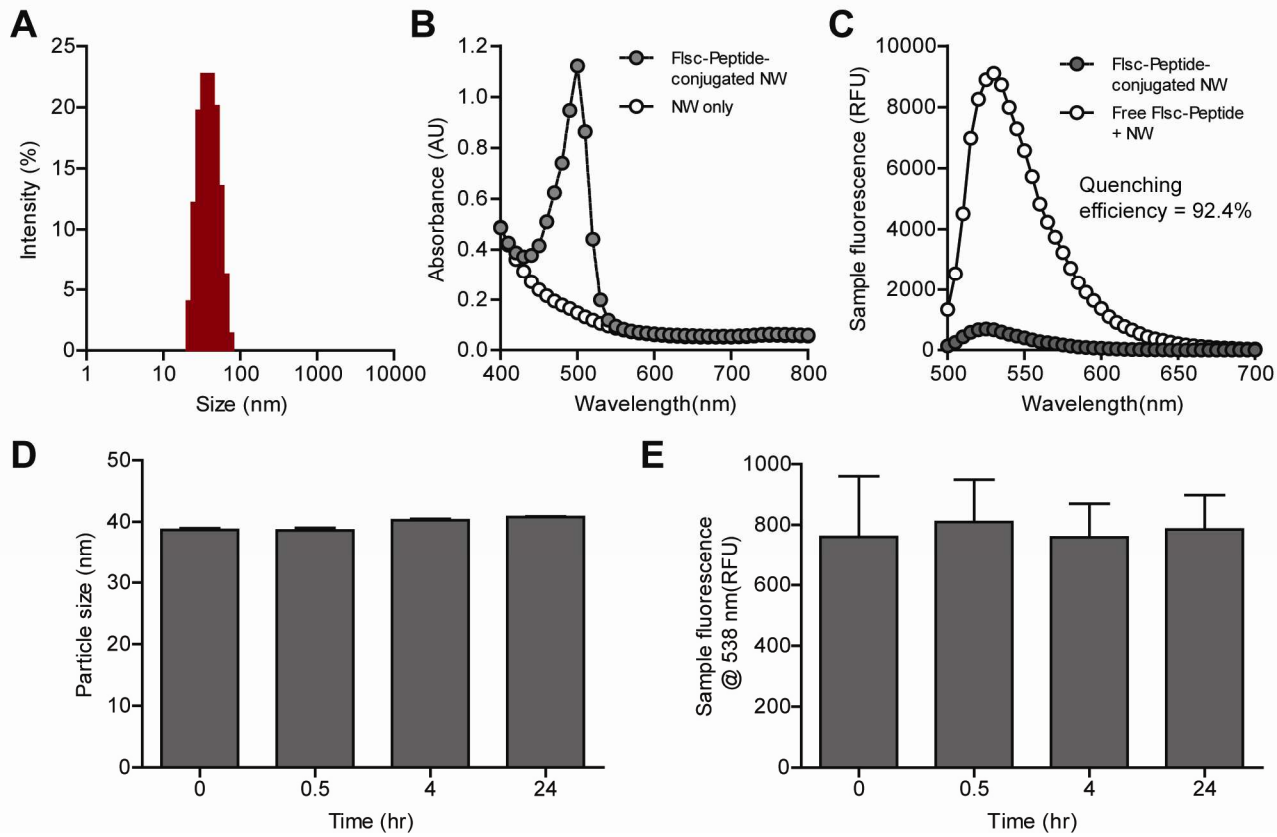

Figure S1. *In vitro* characterization of NWs. (A) Size distribution of iron oxide NWs as determined by dynamic light scattering. (B) Absorbance spectra of NWs conjugated with fluorescein-labeled peptides (~500 nm) and free NWs (white). (C) Fluorescence spectra of NWs conjugated with fluorescein-labeled peptides and NWs incubated with equivalent amount of free fluorescein-labeled peptides (Excitation: 470 nm; emission: 500-700 nm; cutoff: 495 nm; quenching efficiency = 92.4%). (D) Average size of NWs incubated in 10% serum at 37ºC over time as determined by dynamic light scattering (n = 3 per condition, s.d.). (E) Average fluorescence of NWs incubated in 10% serum at 37ºC over time (Excitation: 485 nm; emission 538 nm; cutoff: 530 nm). NWs do not appear to dequench under these conditions (n = 3 per condition, s.d.).

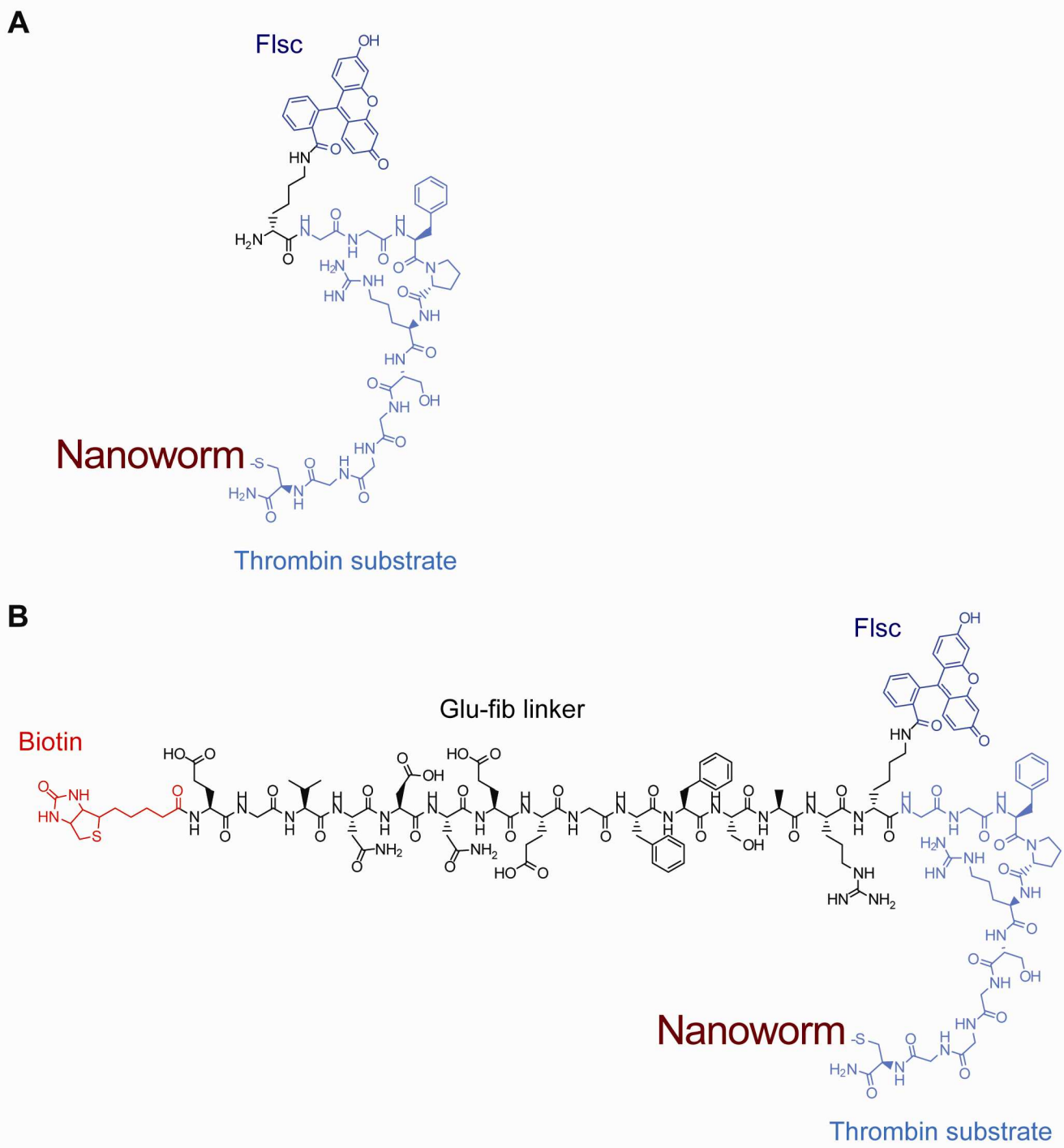

Figure S2. Structures of peptide-conjugated NWs. (A) (K-Flsc)GGfPRSGGGC conjugated to NWs for *in vitro* protease assays. (B) Biotin-eGvndneeGffsar(K-Flsc)GGfPRSGGGC conjugated to NWs for urinary monitoring of thrombosis (Biotin = red, Glu-Fib = black, Flsc = purple, thrombin substrate = blue, NW = brown).

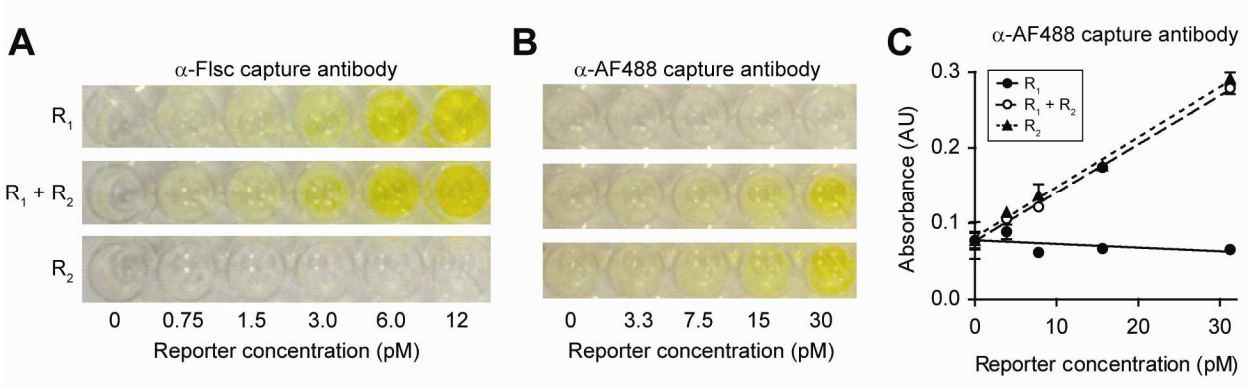

Figure S3. Photograph of developed 96-well plates showing serial dilutions of R1, R1 + R2, and R2 in urine detected using an (A) anti-Flsc or (B) anti-AF488 capture antibody. (C) Absorbance values (λ = 450 nm) of wells coated with anti-AF488 antibodies used to detect serial dilutions of R_1, $R_1 + R_2$, and R_2 in urine (n = 3 per condition, s.d.).

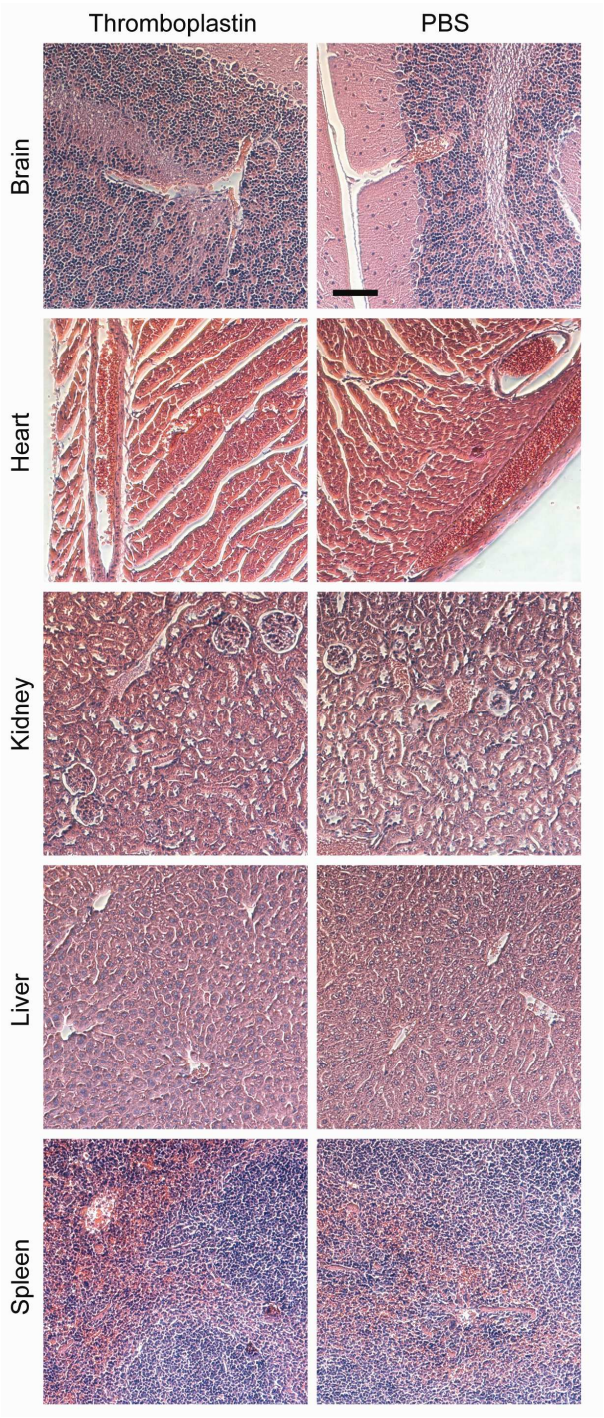

Figure S4. Hematoxylin and eosin staining of organ sections excised from mice following intravenous injection of thromboplastin (2 μL/g b.w.) or PBS (scale bar = 100 μm). No fibrin clots were observed in any of the organ sections.

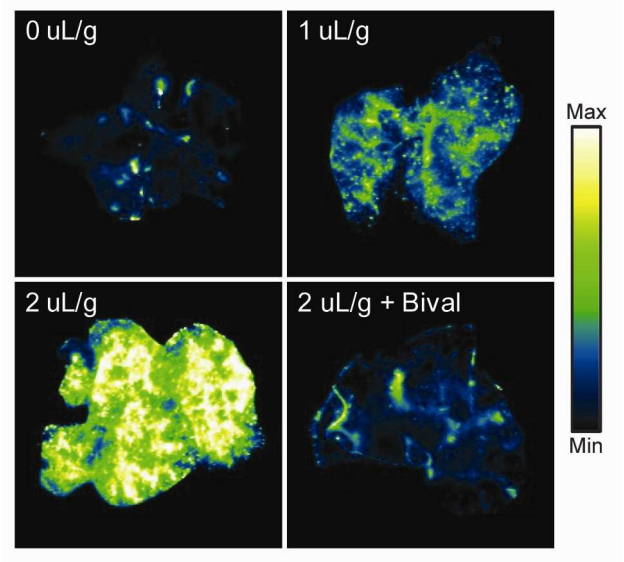

Figure S5. Near-infrared fluorescent scans of the level of VT750-fibrin(ogen) deposited in the lungs in response to increasing doses of thromboplastin and its inhibition by bivalirudin (Bival).

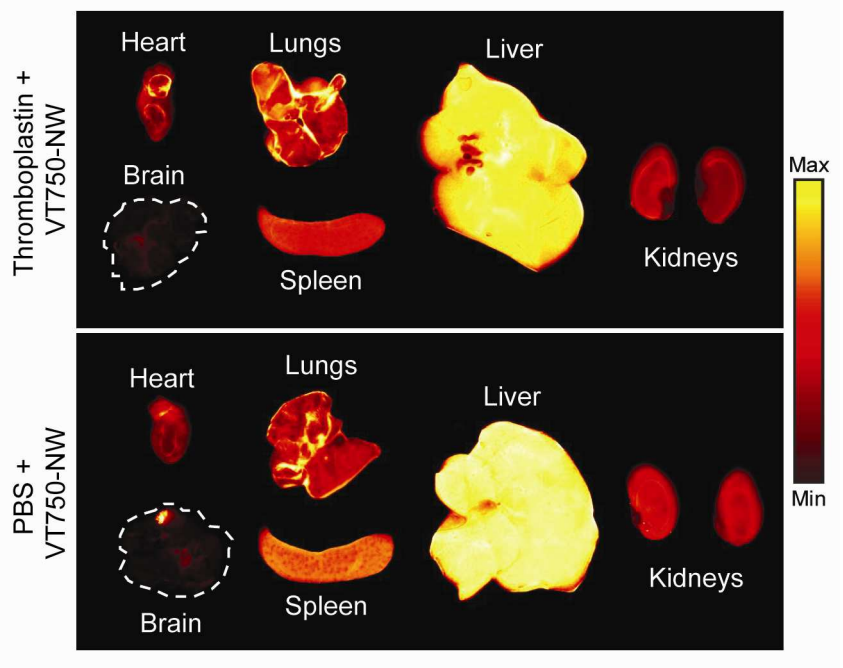

Figure S6. Near-infrared fluorescent scans of excised organs to assess VT750-NW distribution following intravenous injection of thromboplastin (2 µL/g b.w.) or PBS.

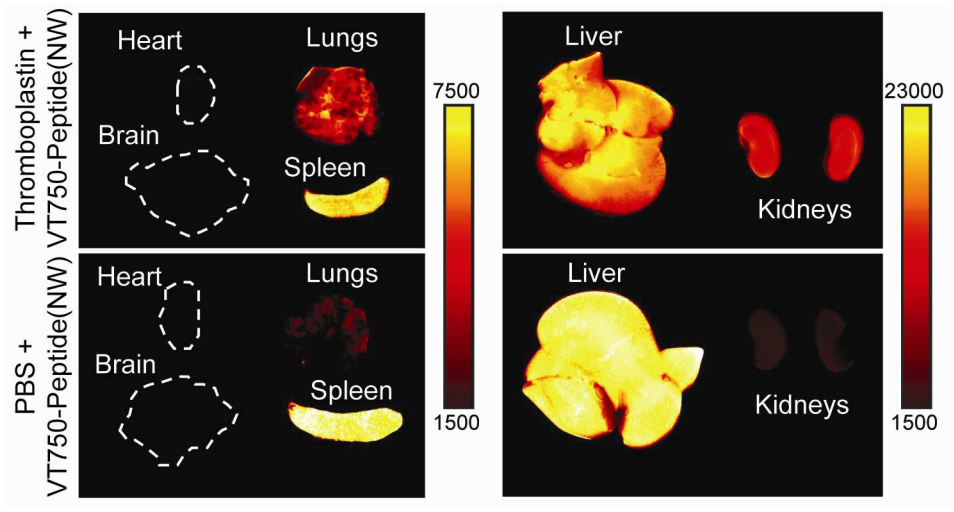

Figure S7. Near-infrared fluorescent scans of excised organs to monitor substrate-NW cleavage in response to thromboplastin (2 μL/g b.w.) or PBS.

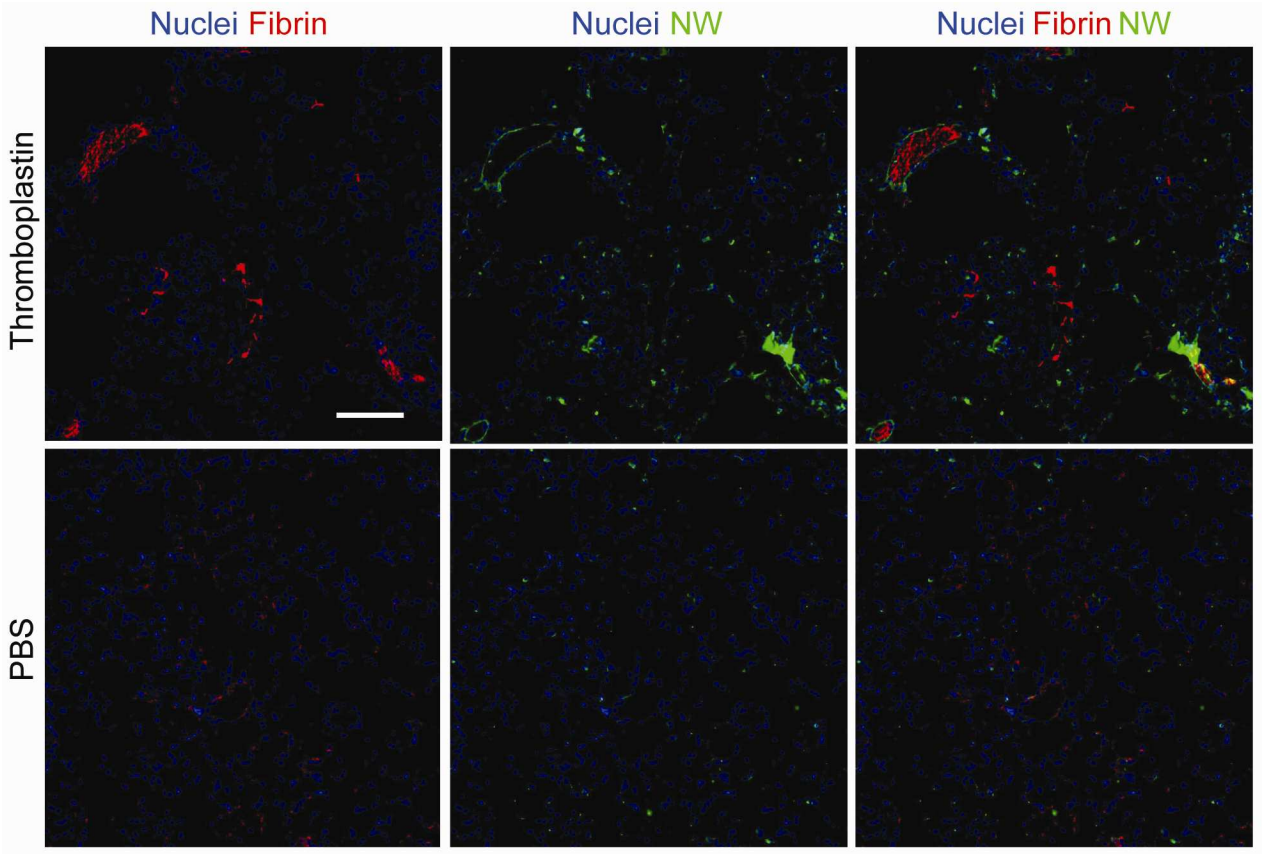

Figure S8. Immunofluorescent staining of lung sections following intravenous injection of thromboplastin or PBS. Staining of fibrin clots (red), NWs (green), and nuclei (blue) in the lung (scale bar = 100 μm).

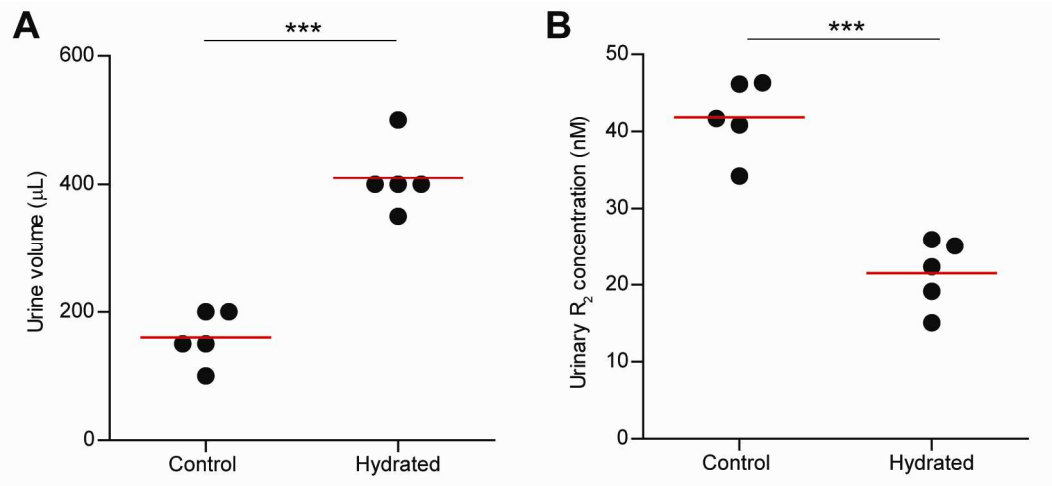

Figure S9. Monitoring urine concentration by administering R_2 intravenously in mice. (A) Urine volume collected from control mice *versus* mice hydrated with 10% body weight equivalent of PBS injected subcutaneously, two hours after administration (***$P < 0.005$, Student's *t*-test; n = 5 mice.). (B) Quantification of R_2 in urine collected from control *versus* hydrated mice *via* ELISA (***$P < 0.005$, Student's *t*-test; n = 5 mice.).